

On the use of Solomon echoes in ^{27}Al NMR studies of complex aluminium hydrides

Bodo Zibrowius^{*,†} and Michael Fischer^{*,‡,¶,§}

[†]*45468 Mülheim an der Ruhr, Germany*

[‡]*Crystallography & Geomaterials, Faculty of Geosciences, University of Bremen,*

Klagenfurter Straße 2-4, 28359 Bremen, Germany

[¶]*Bremen Center for Computational Materials Science, University of Bremen, 28359*

Bremen, Germany

[§]*MAPEX Center for Materials and Processes, University of Bremen, 28359 Bremen,*

Germany

E-mail: bodo.zibrowius@posteo.de; michael.fischer@uni-bremen.de

Abstract

The quadrupole coupling constant C_Q and the asymmetry parameter η have been determined for two complex aluminium hydrides from ^{27}Al NMR spectra recorded for stationary samples by using the Solomon echo sequence. The thus obtained data for KAlH_4 ($C_Q = (1.30 \pm 0.02)\text{ MHz}$, $\eta = (0.64 \pm 0.02)$) and NaAlH_4 ($C_Q = (3.11 \pm 0.02)\text{ MHz}$, $\eta < 0.01$) agree very well with data previously determined from MAS NMR spectra. The accuracy with which these parameters can be determined from static spectra turned out to be at least as good as via the MAS approach. The experimentally determined parameters (δ_{iso} , C_Q and η) are compared with those obtained from DFT-GIPAW (density functional theory - gauge-including projected augmented wave) calculations. Except for the quadrupole coupling constant for KAlH_4 , which is

overestimated in the GIPAW calculations by about 30%, the agreement is excellent. Advantages of the application of the Solomon echo sequence for the measurement of less stable materials or for *in-situ* studies are discussed.

Introduction

Complex aluminium hydrides have been studied rather extensively in the past two decades, mainly because of their potential application as hydrogen storage materials. Triggered by the seminal paper by Bogdanović and Schwickardi,¹ the reversible dehydrogenation of NaAlH_4 under the influence of catalysts was the target of many experimental and theoretical studies. In the course of these investigations, a large number of materials containing aluminium hydrides have been proposed for the reversible storage of hydrogen. Several new complex aluminium hydrides have been discovered and characterized. The progress in this research area has regularly been reviewed from different perspectives.²⁻¹⁰

Beside diffraction methods, NMR spectroscopy has been proven to be a valuable tool for the identification and quantification of the various aluminium hydrides that might be present in the samples under study.¹¹⁻²⁵ Most of the ^{27}Al NMR spectra reported for aluminium hydrides were recorded under MAS conditions, i.e. for samples spinning fast around an axis that is inclined by an angle of $54^\circ 44'$ relative to the direction of the magnetic field. This technique is one of the standard methods to tackle the resolution problems in solid-state NMR spectroscopy. It significantly reduces the line broadening caused by second-order quadrupole interaction and removes the broadening brought about by the heteronuclear dipole-dipole interaction as well as by the anisotropy of the chemical shift.²⁶ The thus enhanced spectral resolution allows the aluminium hydride species to be identified by the position of the centreband of the central transition. It should be noted that there are cases where this approach is bound to fail. If the quadrupole interaction is as strong as for instance recently found for the aluminium nuclei in $\text{Mg}(\text{AlH}_4)_2$ ²⁷ or in an alane amine adduct,²⁸ the static linewidth of the central transition at the usually available magnetic fields exceeds the available spinning

speeds by far. Nevertheless, ^{27}Al NMR spectra can be recorded for non-spinning samples by an echo technique and can be used to characterize these materials.

Quadrupole interaction should not so much be regarded as an obstacle for recording highly resolved NMR spectra of solids, but first and foremost as a valuable source of information difficult to be gathered by other means. Any nucleus with a spin $I > \frac{1}{2}$ has a non-vanishing electric quadrupole moment that interacts with the electric field gradient (efg) at the site of the nucleus. This interaction influences the NMR frequency of the nucleus studied. Hence, any quadrupole nucleus can be regarded as a probe of the local geometry in general and of the symmetry in particular. Apart from the orientation of its principal axes system, the quadrupole coupling can be fully described by just two parameters: the so-called quadrupole coupling constant C_Q , which is proportional to both the strength of the gradient and the electric quadrupole moment of the nucleus under study, and the asymmetry parameter η of the efg.^{26,29,30} For example, if the nucleus is located on a symmetry axis C_n with $n \geq 3$, the efg is axially symmetric and η is zero. In a cubic environment, there is no gradient and hence there is no quadrupole interaction.

For materials where the quadrupole interaction is small (or medium sized), the second-order quadrupolar broadening of the central transition is hardly noticeable or causes only a small splitting of a few ppm in the ^{27}Al MAS NMR spectra. However, these spectra contain much more information than only the isotropic chemical shift. The range over which the spinning sidebands of the satellite transitions spread and the characteristic intensity modulations of these sidebands allow the parameters of the quadrupole interaction to be determined very precisely. This has been shown for NaAlH_4 ¹⁸ and KAlH_4 .²⁵

The major aim of the present paper is to demonstrate that the information about the chemical shift and the quadrupole interaction can alternatively be gained from ^{27}Al NMR spectra obtained from Solomon echoes recorded for non-spinning samples. Although the formation of these echoes was demonstrated for the first time more than 60 years ago³¹ and their origin is well understood,^{32,33} Solomon echoes have rarely been used to observe

the satellite transitions in solid-state ^{27}Al NMR spectroscopy.³⁴ The precision of NMR data obtained from stationary samples is generally assumed to be lower than of those derived from MAS NMR spectra. However, this approach avoiding fast sample spinning is certainly advisable for less stable materials that are prone to decomposition under mechanical and/or thermal stress.

With the above discussed high sensitivity of the quadrupole interaction to the local environment of the nucleus, the precise determination of the quadrupole coupling parameters combined with DFT (density functional theory) calculations can offer an alternative approach to high-quality structures for polycrystalline materials.³⁵ We show that the experimental data obtained for NaAlH_4 and KAlH_4 are well reproduced by DFT-GIPAW (gauge-including projected augmented wave) calculations.³⁶

Experimental and computational methods

Materials

NaAlH_4 (Chemetall, 82–85%) was purified by dissolving it in tetrahydrofuran and filtrating off the insoluble portions. The pure NaAlH_4 was precipitated from the solution by addition of pentane and carefully dried in vacuum.

KAlH_4 was produced by ball milling NaAlH_4 and KCl .²⁵ The resulting powder was suspended in diglyme. After filtration, KAlH_4 was precipitated through the addition of toluene and filtered off. The dried KAlH_4 contained small amounts of unreacted NaAlH_4 which were removed by treatment in tetrahydrofuran.

All syntheses and operations were performed under argon using dried and oxygen-free solvents. The MAS rotors were filled and capped in a glove box and transferred to the spectrometer in argon-filled vials.

Solid-state NMR spectroscopy

The ^{27}Al NMR spectra were recorded on a Bruker Avance III HD 500WB spectrometer using double-bearing MAS probes (DVT BL4) at resonance frequencies of 130.3 MHz. The chemical shift was referenced relative to an external 1.0 M aqueous solution of aluminium nitrate. The same solution was used for determining the flip-angle.

For the ^{27}Al MAS NMR spectra, single $\pi/12$ pulses ($t_p = 0.6 \mu\text{s}$) were applied at a repetition time of 2 s (2,000–16,000 scans) and spinning frequencies (ν_{MAS}) between 3 and 13 kHz. High-power proton decoupling (SPINAL-64) was used for all ^{27}Al NMR spectra shown in this paper. The magic angle was adjusted by maximizing the rotational echoes of the ^{23}Na resonance of solid NaNO_3 .

The ^{27}Al NMR spectra of stationary samples were acquired using the Solomon echo sequence with two pulses of the same length t_p separated by a delay τ .³¹ For all half-integer spins with $I > \frac{3}{2}$, this pulse sequence generates in general a whole series of echoes. For ^{27}Al ($I = \frac{5}{2}$), echoes at τ , 2τ , and 3τ after the second pulse are expected for the inner satellite transitions ($(+\frac{1}{2} \leftrightarrow +\frac{3}{2})$ and $(-\frac{3}{2} \leftrightarrow -\frac{1}{2})$) and at $\tau/2$, τ , and $3\tau/2$ for the outer satellite transitions ($(+\frac{3}{2} \leftrightarrow +\frac{5}{2})$ and $(-\frac{5}{2} \leftrightarrow -\frac{3}{2})$).³² The echoes at $\tau/2$, τ , and 2τ are referred to as allowed echoes and those at 3τ and $3\tau/2$ are referred to as forbidden echoes.^{31–33} Which of the various echoes are experimentally observed can to a certain extent be influenced by the phase cycling applied.³⁷ The echo at τ that is used here to obtain the spectra contains the spectral information of both satellite transitions. Solomon echoes can be generated with two in-phase pulses ($p_x-\tau-p_x-\tau-\text{acq}$) or two pulses in quadrature phase ($p_x-\tau-p_y-\tau-\text{acq}$).^{32,38} Combining both variants with phase alternation of the second pulse and CYCLOPS (CYCLically Ordered Phase Sequence³⁹) yields the 16-step phase cycle that was originally proposed by Kunwar et al.⁴⁰ This phase cycle, which is known to effectively cancel spurious signals from the NMR probe,³⁸ was used for the acquisition of all Solomon echo data shown here.

Solomon echoes that were obtained in this way for KAlH_4 with various pulse spacings τ

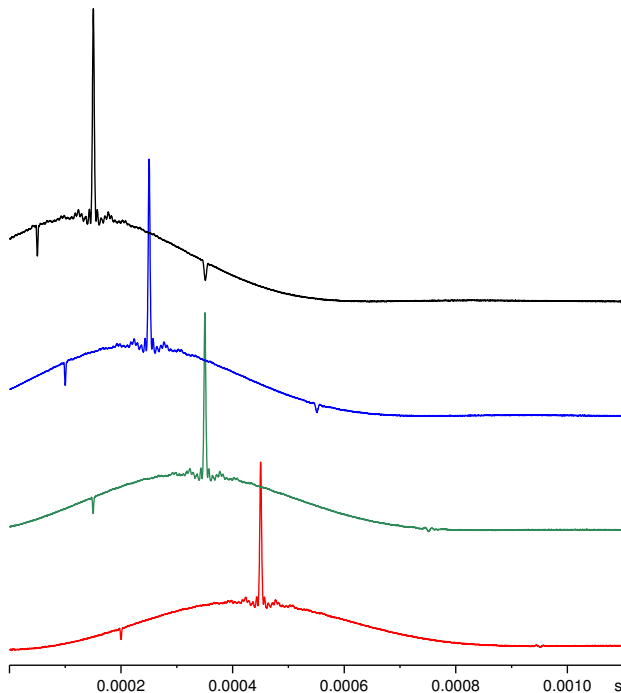


Figure 1: ^{27}Al NMR Solomon echoes generated for KAlH_4 by applying two pulses ($t_p = 0.9 \mu\text{s}$) separated by 200, 300, 400, and $500 \mu\text{s}$ (from top to bottom). For recording these echoes, a short pre-acquisition delay of only $50 \mu\text{s}$ was used.

are shown in Fig. 1. The additional echoes at $\tau/2$ and 2τ can easily be discerned. The echo at $\tau/2$ is narrower than the other two since it contains only the spectral information from the wider outer satellite transition. Obviously, the forbidden echo at $3\tau/2$ is not observed under the experimental conditions chosen. This also holds true for the forbidden echo at 3τ . The existence of several echoes for nuclei with $I \geq \frac{5}{2}$ is generally regarded as a main drawback of this technique since Fourier transform of the time signal generally leads to distorted spectra, necessitating a direct analysis of the echoes in the time domain.³³

To minimize the interfering effect of the echo generated at 2τ after the second pulse, we generally used pulse spacings τ of at least 0.5 ms. For both KAlH_4 and NaAlH_4 , intense echoes at τ could be obtained for pulse spacings up to 1.2 ms. Since Solomon echoes can only be observed if the pulse spacing is much smaller than the duration of the free induction decay of the central transition (T_{FID}),^{32,33} the rather slow spin-spin relaxation in these two aluminium hydrides is obviously a fortunate circumstance for the application of this

technique.

For the spectra shown here, two strong rf pulses ($\nu_{rf} \approx 100$ kHz) with a length $t_p = 0.9 \mu\text{s}$ were applied. With a repetition time of 2 s, between 16,000 and 48,000 scans were accumulated. To start Fourier transform at the top of the echo at τ , a pre-acquisition delay slightly shorter than τ and an appropriate number of left shifts were applied (dwell time: $0.05 \mu\text{s}$).

The spectra simulations were performed using the solids lineshape analysis module implemented in the TopSpinTM 3.2 NMR software package from Bruker BioSpin GmbH.

DFT-GIPAW calculations

All DFT calculations were carried out using the CASTEP code.^{41,42} The calculations employed the PBE exchange-correlation functional,⁴³ using ultrasoft pseudopotentials generated on the fly and a plane wave cutoff energy of 800 eV. The structures of NaAlH₄ and KAlH₄ were optimized, relaxing all atomic positions while fixing the unit cell parameters to experimental values. The optimizations, which employed a BFGS optimizer, were considered converged when the maximal residual force on an atom fell below 0.001 eV/Å and when the maximal atomic displacement with respect to the previous step was smaller than 0.0005 Å.

The starting structure of NaAlH₄ was taken from the work of Hauback et al. (space group $I4_1/a$, $a = 5.0119$ Å, $c = 11.3147$ Å).⁴⁴ The alternative use of the structural data published by Ozolins et al. (space group $I4_1/a$, $a = 5.0099$ Å, $c = 11.3228$ Å)⁴⁵ led to essentially identical results. A $7 \times 7 \times 3$ mesh of k -points, corresponding to 26 irreducible points, was used to sample the first Brillouin zone. For KAlH₄, the atomic coordinates were taken from a previous neutron diffraction study of KAlD₄,⁴⁶ whereas cell parameters were taken from the more recent X-ray diffraction study of KAlH₄ by Zibrowius and Felderhoff (space group $Pnma$, $a = 8.8475$ Å, $b = 5.8143$ Å, $c = 7.3448$ Å).²⁵ For this structure, a $4 \times 6 \times 5$ mesh of k -points, corresponding to 18 irreducible points, was used.

DFT calculations of the isotropic shielding parameter σ_{iso} , the quadrupole coupling con-

stant C_Q , and the asymmetry parameter η employed the gauge-including projector augmented wave (GIPAW) method as implemented in CASTEP.^{36,47–49} Calculations were performed on the DFT-optimized structures, as a prior optimization of the atomic coordinates obtained from diffraction data is crucial to obtain meaningful results for hydrogen-containing systems. Even when neutron diffraction is used, a highly accurate determination of the hydrogen positions is challenging. Inaccuracies in the hydrogen positions result in large errors in the calculated NMR parameters.^{36,50,51} In terms of exchange-correlation functional, pseudopotentials, cutoff energy, and k -meshes, the same settings as for the optimisation were used for the DFT-GIPAW calculations. The analysis of the calculated NMR parameters made use of the MagResView tool.⁵²

In order to compare the isotropic magnetic shielding $\sigma_{iso,DFT}$ directly obtained from the DFT-GIPAW computations with the experimentally accessible chemical shift data, a conversion to $\delta_{iso,DFT}$ is required. In the first place, such a conversion was made by using LiAlH_4 as the sole reference system. Calculations analogous to those described above were carried out for LiAlH_4 , using the crystal structure of LiAlD_4 reported by Hauback et al.⁵³ as starting point (k -mesh: $8 \times 5 \times 5$). The chemical shift of the systems of interest was then calculated as:

$$\delta_{iso,DFT,1} = 454.8 \text{ ppm} + 102.0 \text{ ppm} - \sigma_{iso,DFT} = 556.8 \text{ ppm} - \sigma_{iso,DFT}, \quad (1)$$

where 454.8 ppm corresponds to the shielding value $\sigma_{iso,DFT}$ calculated for LiAlH_4 and 102.0 ppm is the isotropic shift experimentally observed with respect to the usual standard.¹¹

To evaluate the performance of the DFT-GIPAW computations across a broader set of systems, additional calculations were carried out for three other alkali aluminium hydrides, namely Li_3AlH_6 (k -mesh: $6 \times 6 \times 4$),⁵⁴ Na_3AlH_6 (k -mesh: $6 \times 6 \times 4$),⁴⁵ and $\text{Na}_2\text{LiAlH}_6$ (k -mesh: $6 \times 6 \times 6$).⁵⁵ The references cited for the structures are combined X-ray and neutron diffraction studies of the corresponding isostructural aluminium deuterides. The experimental data for

δ_{iso} of Li_3AlH_6 were taken from Wiench et al.¹⁵ and those for Na_3AlH_6 and $\text{Na}_2\text{LiAlH}_6$ from Zhang et al.¹⁸

It should be noted that there are two non-equivalent Al atoms in the rhombohedral crystal structure reported for Li_3AlH_6 by Brinks and Hauback.⁵⁴ In particular, because of the results of a detailed analysis carried out by Løvvik et al.,^{56,57} we regard this structural solution as rather convincing. Surprisingly, only a single resonance line was observed in the NMR spectrum of Li_3AlH_6 .¹⁵ Our calculations yield a clue to explain this apparent discrepancy. For the magnetic shielding $\sigma_{iso,DFT}$ of Al1 and Al2 in Li_3AlH_6 , we obtained 600.2 ppm and 602.7 ppm, respectively. The results for the quadrupole coupling constant C_Q are 2.54 MHz and -1.54 MHz for Al1 and Al2, respectively. For symmetry reasons, the asymmetry parameter is $\eta = 0$ for both positions. We assume that the experimentally determined values $\delta_{iso} = -33.7$ ppm and $C_Q = 1.4$ MHz can be assigned to Al2. According to our calculations, Al1 should give rise to a resonance line about 2.5 ppm downfield of the line of Al2. However, the much stronger quadrupole coupling leads to a more significant second-order broadening and to a more pronounced quadrupole-induced highfield shift. At the resonance frequency of 104 MHz used by Wiench et al.,¹⁵ the centres of gravity of both resonance lines are expected to be only 0.2 ppm apart of each other. Furthermore, it has to be taken into account that the Li_3AlH_6 studied by these authors was produced by ball-milling LiAlH_4 and LiH . Immediate products of mechanochemical syntheses very often have a rather poor crystallinity. This seems to be the case for Li_3AlH_6 produced via ball milling as the results of a study devoted to this solid-state phase transformation show.⁵⁸ The resolution of the X-ray powder pattern for the obtained product was insufficient to determine the space group. Fig. S1 in the Supporting Information demonstrates that under these circumstances the resonance line of Al1 would be hardly visible. A high-field NMR investigation using well crystallized material should be able to verify our hypothesis.

To establish an equation to convert the shielding $\sigma_{iso,DFT}$ into chemical shifts $\delta_{iso,DFT}$, a linear regression was computed across all six systems. Literature data for δ_{iso} of the two

hydrides studied here, NaAlH_4 and KAlH_4 , were included in the regression.^{18,25} The data points as well as the linear fit are shown in Fig. 2. The resulting equation for the conversion is:

$$\delta_{iso,DFT,1} = 514.3 \text{ ppm} - 0.9064 \cdot \sigma_{iso,DFT}. \quad (2)$$

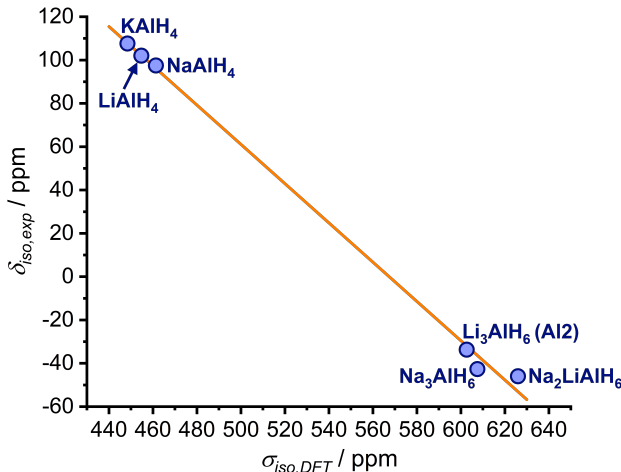


Figure 2: Experimentally determined ^{27}Al chemical shifts δ_{iso} vs isotropic shieldings σ_{iso} obtained from the DFT-GIPAW computations for some alkali aluminium hydrides. The squared correlation coefficient R^2 of the fit is 0.997.

Results and Discussion

Experimental results for KAlH_4

Fig. 3 shows a ^{27}Al NMR spectrum obtained as a Fourier transform of the Solomon echo (formed at τ after the second pulse) for a stationary KAlH_4 sample in comparison with the best fit. The depicted lineshape is typical of a first-order quadrupolar broadened powder spectrum.³⁰ The positions of the characteristic discontinuities of the lineshape are obviously nicely reproduced by the fit. The significantly reduced intensity in the outer wings of the experimental spectrum is mainly caused by the insufficient excitation width of the finite pulses used.⁵⁹ Neither the finite excitation width nor the finite bandwidth of the NMR probe are taken into account by the simulation program used. It should be noted that the

resonance line of the central transition is not caused by the Solomon echo but by the free induction decay following the second pulse of the pulse sequence.³³

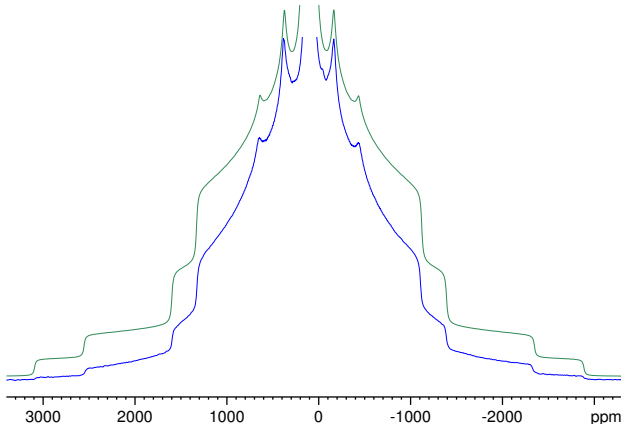


Figure 3: Experimental ^{27}Al NMR spectrum of KAlH_4 obtained from a Solomon echo generated with a pulse spacing of $600\ \mu\text{s}$ (blue) and the best fit of this spectrum (green) using the following parameters: $\delta_{iso} = 108\ \text{ppm}$, $C_Q = 1.30\ \text{MHz}$ and $\eta = 0.64$. For the experimental spectrum, a Lorentzian line broadening with $LB = 1200\ \text{Hz}$ was applied to suppress small modulations caused by the echo at 2τ that was still noticeable despite the long pulse spacing used. The spectrum is cut off at about 6% of the maximum intensity of the central line. For the simulated spectrum, a Lorentzian line broadening with $LB = 2000\ \text{Hz}$ was applied.

The fact that such a complex resonance line can be described by only three parameters is somewhat amazing: the position of the line is mainly determined by the isotropic chemical shift δ_{iso} and its shape is governed by the quadrupole coupling constant C_Q and the asymmetry parameter η .³⁰ The latter two parameters also have a small but significant effect on the line position via the quadrupole induced shift δ_{qis} .⁶⁰ This second-order effect that is inversely proportional to the square of the magnetic field applied influences the centre of gravity of the central transition and each pair of satellite transitions in a characteristic way. Hence, the line position read off a spectrum must generally be corrected to obtain the true chemical shift for any half-integer quadrupolar nucleus. Simulation programs take the quadrupole induced shift into account.

It should be noted that from the NMR measurements reported here, only the magnitude, but not the sign of the quadrupole coupling constant C_Q can be determined. The resonance lines of every pair of satellite transitions are mirror images of each other. In accordance with

most of the NMR literature,²⁹ we omit the absolute value bars for C_Q throughout the paper.

To have a suitable simulation program at hand is useful, but not essential for determining the spectral parameters from experimental spectra measured for stationary samples. In fact, rather good estimates of these parameters can directly be read off the experimental spectrum in Fig. 3. The maxima of the inner satellite transitions at 380 and -162 ppm yield a value of 109 ppm for the centre of gravity of these transitions. Since for any nucleus with $I = \frac{5}{2}$, the position of the centre of gravity of the inner satellite transitions is known to be much closer to the isotropic chemical shift than the centre of gravity of the central transition,⁶⁰ this estimate is very close to the true isotropic chemical shift $\delta_{iso} = (108 \pm 2)$ ppm found by means of the simulation program.

The quadrupole coupling constant C_Q can be derived from the total spread of the satellite transitions $\Delta\nu_{TS}(m)$. For the inner satellite transitions ($m = \frac{3}{2}$), the following relation holds:^{25,59,61}

$$C_Q = \frac{10}{3} \Delta\nu_{TS}(\frac{3}{2}). \quad (3)$$

Since the outermost shoulders of the inner satellite transitions are localized at 1610 ppm (low-field) and -1390 ppm (high-field), we have a total spread of 3000 ppm corresponding to $\Delta\nu_{TS}(\frac{3}{2}) \approx 390$ kHz. With eqn (3), this value leads to the rather good estimate of $C_Q \approx 1.3$ MHz. The asymmetry parameter can be estimated from the ratio of the splitting of the maxima $\Delta\nu_M(m)$ to the total spread of any pair of satellite transitions according to the following equation:²⁵

$$\eta = 1 - \frac{2\Delta\nu_M(m)}{\Delta\nu_{TS}(m)}. \quad (4)$$

With the above given values for the positions of the maxima of the inner satellite transitions, we find a splitting of 542 ppm corresponding to $\Delta\nu_M(\frac{3}{2}) \approx 71$ kHz. With eqn (4), we obtain $\eta \approx 0.64$. Of course, the quadrupole parameters can also be obtained from the outer satellite transitions, but the discontinuities are usually much better defined for the narrower inner satellite transitions. The estimates for C_Q and η turned out to be so precise that they could

not be improved by means of the simulation program. We think that the margins of error given for C_Q (± 20 kHz) and η (± 0.02) in Table 1 are rather conservative estimates. Hence, the reliability of determining the parameters of the quadrupole coupling for KAlH_4 from static spectra is as good as that from spectra measured under MAS conditions.²⁵ Regarding the accuracy of the determination of the isotropic chemical shift, the MAS approach is definitely superior.

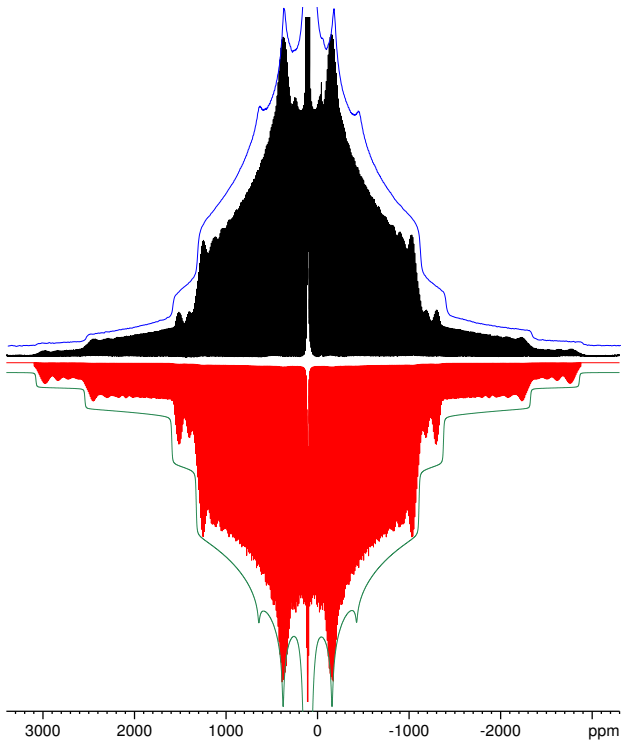


Figure 4: Experimental ^{27}Al NMR spectra of measured for a stationary sample (blue) and the same sample spinning at $\nu_{MAS} = 1.4$ kHz (black) and their simulations (green and red, respectively) with the parameters $\delta_{iso} = 107.6$ ppm, $C_Q = 1.29$ MHz and $\eta = 0.64$. To ease the comparison, the simulated spectra have been inverted.

Fig. 4 compares the ^{27}Al NMR spectra measured with and without MAS with the simulated spectra using the parameters previously determined from MAS spectra measured at different spinning speeds. The quality of the fits can better be judged from the enlarged version of Fig. 4 given as Fig. S2 in the Supporting Information. Amazingly, the tiny amount of the cryolite-like by-product Na_3AlH_6 detected as narrow line at -42.7 ppm in the MAS NMR spectrum²⁵ can also be identified as shoulder at about -40 ppm in the static spectrum.

Although the lineshape simulations neglect the effect of a possible anisotropy of the chemical shift, they reproduce the experimental lineshapes quite well. Hence, any anisotropy must be rather small and contributes only to the line broadening of the static spectrum. This observation is in line with the results of our GIPAW calculations. For the span Ω , a parameter describing the total spread of a resonance line governed by chemical shift anisotropy,⁶² these calculations yield a value of 11 ppm corresponding to less than 1.5 kHz (see Supporting Information, Table S1).

Experimental results for NaAlH₄

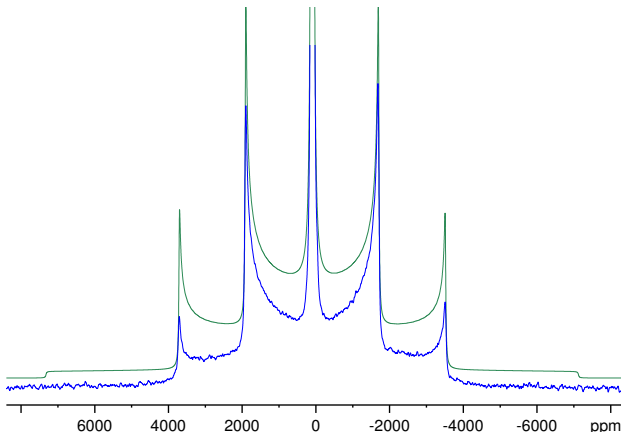


Figure 5: Experimental ^{27}Al NMR spectrum of NaAlH_4 obtained from a Solomon echo generated with a pulse spacing of $600\ \mu\text{s}$ (blue) and the best fit of this spectrum (green) using the following parameters: $\delta_{iso} = 99\ \text{ppm}$, $C_Q = 3.11\ \text{MHz}$ and $\eta = 0$. Lorentzian line broadening with $LB = 3000\ \text{Hz}$ and $LB = 4000\ \text{Hz}$ was applied for the experimental spectrum and the simulated spectrum, respectively. The experimental spectrum is cut off at about 12% of the maximum intensity of the central line.

Fig. 5 shows a ^{27}Al NMR spectrum obtained as a Fourier transform of the Solomon echo for a stationary NaAlH_4 sample in comparison with the best fit. Again, the lineshape is typical of a first-order quadrupolar broadened powder spectrum, but this time for the case of an axially symmetric electric field gradient tensor, i.e. $\eta = 0$.^{26,30,59} Apart from the central transition, the spectrum shows the sharp maxima of the four satellite transitions. These maxima correspond to the perpendicular components of the axially symmetric efg tensor.

The maxima of the inner satellite transitions are found at about 1887 and -1674 ppm, corresponding to a splitting of the maxima $\Delta\nu_M(\frac{3}{2})$ of about 464 kHz. Since, for $\eta = 0$, the total spread $\Delta\nu_{TS}(m)$ equals $2\Delta\nu_M(m)$ (see eqn (4)), we obtain with eqn (3) a value of $C_Q \approx 3.09$ MHz as an estimate of the strength of the quadrupole coupling. Using the simulation program, we found for the best fit $C_Q = 3.11$ MHz.

As expected from the known structure of NaAlH_4 ,^{44,45} we found no indication for a deviation from axial symmetry. Since the Al atoms are located in Wyckoff position 4b, i.e. on a C_4 axis, the asymmetry parameter η is bound to be zero. However, with the finite linewidth observed, it is difficult to verify experimentally that $\eta = 0$ holds. From our experimental data, we can safely deduce that $\eta < 0.01$ is the upper bound for a deviation from axial symmetry.

Because of the enormous width of the spectrum, the deviations of the experimental from the simulated lineshape are more pronounced than in the case of KAlH_4 . From the above given splitting of the maxima of the inner transition $\Delta\nu_M(\frac{3}{2})$, it follows that the total spread of the outer satellite transition $\Delta\nu_{TS}(\frac{5}{2})$ is about 1.86 MHz. In particular, the shoulders of the outer satellite transition can not be discerned in the experimental spectrum. However, these distortions of the lineshape are less severe than for spectra obtained from the free induction decay after a single pulse. During the inevitable receiver dead time after the pulse, the fast decaying signal corresponding to the broad features is lost and only the sharp maxima can be seen in these spectra.^{12,19} It seems unlikely that this approach could produce meaningful results for the quadrupole parameters for the general case $\eta \neq 0$. In our own attempts to record ^{27}Al NMR spectra for stationary NaAlH_4 samples by single pulse excitation, we ran into serious phasing problems.

Fig. 6 compares the ^{27}Al NMR spectra measured with and without MAS with the simulated spectra using the parameters determined from MAS spectra measured at different spinning speeds. The quality of the fits can better be judged from the enlarged version of Fig. 6 given as Fig. S3 in the Supporting Information. As for KAlH_4 , we do not see any of

the characteristic effects of a possible anisotropy of the chemical shift in the spectra recorded for stationary samples or under MAS conditions. Our GIPAW calculations yield a value of about 19 ppm for the span Ω , corresponding to about 2.5 kHz.

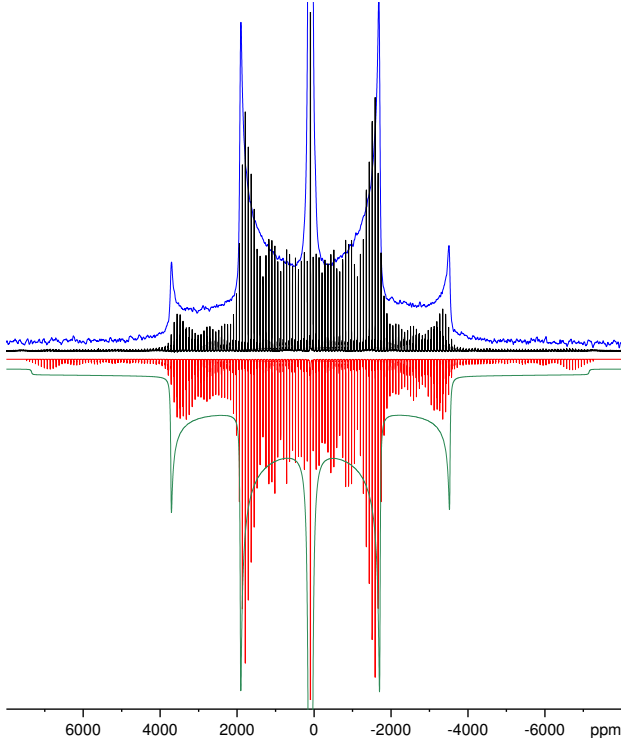


Figure 6: Experimental ^{27}Al NMR spectra of NaAlH_4 measured for a stationary sample (blue) and the same sample spinning at $\nu_{MAS} = 10$ kHz (black) and their simulations (green and red, respectively) with the parameters $\delta_{iso} = 97.2$ ppm, $C_Q = 3.11$ MHz and $\eta = 0$. To ease the comparison, the simulated spectra have been inverted.

As distinct from the case of KAlH_4 at the same field strength,²⁵ the effect of second-order quadrupole interaction is not fully masked by other broadening mechanisms. The centreband of the central transition shown in Fig. 7 exhibits two maxima separated by about 3 ppm (95.6 and 92.3 ppm). These maxima are best resolved at spinning rates between 3 and 6 kHz. We assume that the reduced resolution at higher spinning rates is caused by frictional heating that leads to a significant increase of the temperature in certain parts of the sample that influences the chemical shift and/or the quadrupole coupling parameters.^{63,64} Fig. 7 also shows that the splitting and the general lineshape of the centreband can nicely be fitted using the same parameters as for the simulated spectra of the satellite transitions in Fig. 6.

However, at the still rather low ratio of the quadrupole coupling constant to the resonance frequency ($C_Q/\nu_L \approx 0.024$), the experimental lineshape of the centreband of the central transition does not really show the discontinuities characteristic for second-order quadrupolar broadening.^{26,30,59} A reliable determination of the parameters of the quadrupole coupling would not be possible. These parameters can be obtained with much higher accuracy from the satellite transitions governed by first-order quadrupole interaction, either from spectra of stationary samples measured by means of the Solomon echo sequence or from the characteristic sideband patterns of MAS spectra measured with single-pulse excitation. Since the second-order broadening is proportional to the square of the quadrupole coupling constant, it can, of course, not deliver any information about the sign of C_Q either.

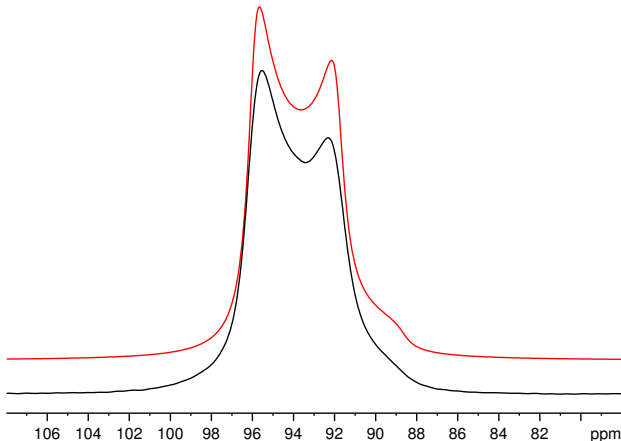


Figure 7: Experimental ^{27}Al NMR spectrum of NaAlH_4 measured at $\nu_{MAS} = 5$ kHz (black) and its simulation (red) with the parameters $\delta_{iso} = 97.2$ ppm, $C_Q = 3.11$ MHz and $\eta = 0$. Only the region of the centreband is shown. Lorentzian line broadening with $LB = 20$ Hz and $LB = 120$ Hz was applied for the experimental spectrum and the simulated spectrum, respectively.

GIPAW vs experiment

The results from the DFT-GIPAW calculations are collected in Table 1, where experimental values from this study and previous work are given for comparison. With regard to the ^{27}Al chemical shifts, both the use of LiAlH_4 as sole reference system (eqn (1)) and the calculation by means of a linear regression over several alkali aluminium hydrides (eqn (2)) deliver very

good agreement with experiment. While the former approach should be suitable for converting DFT-computed chemical shieldings into chemical shifts for structurally closely related systems, the regression-based approach can be expected to be more broadly applicable for diverse alkali aluminium hydrides. The direct results of the DFT-GIPAW calculations (C_Q , η , σ_{ii}) for all substances mentioned are summarised in Table S1 (Supporting Information).

The DFT-GIPAW quadrupole coupling constant C_Q of KAlH_4 is approximately 30% (0.4 MHz) larger than the experimental values. A similar overestimation was found in a previous DFT-GIPAW study of Na_3AlH_6 .¹⁸ In that study, the observed difference was attributed to the influence of thermal motion on the electric field gradients, which is not taken into account in static DFT calculations. In contrast, our calculated quadrupole coupling constant for NaAlH_4 is in perfect agreement with the experimental one. It is important to note that our procedure is different from that applied by Zhang et al.¹⁸ These authors used the experimentally determined value for C_Q and the calculated field gradient of NaAlH_4 to determine the quadrupole moment $Q(^{27}\text{Al})$. The thus obtained quadrupole moment was then used to calculate the quadrupole couplings for the other aluminates investigated. Our calculations of the parameters of the quadrupole interaction are solely based on the crystallographic data and the generally accepted value of the quadrupole moment $Q(^{27}\text{Al}) = 146.6$ mbarn.⁶⁵ Hence, the calculated data reported here are fully independent from our experimental data.

Recently, a slightly higher value of the quadrupole moment $Q(^{27}\text{Al}) = 148.2$ mbarn was recommended on the basis of highly accurate coupled cluster calculations with single, double, and perturbative triple excitations [CCSD(T)] for Al-containing molecules.⁶⁶ By using this value, the magnitudes of the calculated quadrupole coupling constants would be about 1% higher than given in Table 1 and Table S1 (Supporting Information). DFT calculations carried out with the newly recommended value for the quadrupole moment typically resulted in C_Q values deviating by about 10 to 15% from experiment.⁶⁶

With regard to the asymmetry parameters, the DFT-calculated $\eta = 0.59$ for KAlH_4 agrees very well with the experimental values, both from the literature and from the present

work. For NaAlH_4 , $\eta = 0$ reflects the high symmetry of the local environment (site symmetry: $\bar{4}$).^{44,45} All four Al–H bonds are equivalent by symmetry.

Although not in the focus of the present paper, we want to mention the GIPAW results for the counterions. We obtained a good agreement between experiment and calculations for the quadrupole parameters for ^{39}K in KAlH_4 : $C_Q = 0.562/0.68$ MHz (Exp.²⁵/GIPAW) and $\eta = 0.74/0.79$. Unfortunately, the result for ^{23}Na in NaAlH_4 is less encouraging: $C_Q = 0.15/-0.46$ MHz (Exp.¹⁸/GIPAW) and $\eta = 0/0$. As mentioned above, we omit the sign of C_Q for the experimental data.

Table 1: Comparison of the results of DFT-GIPAW calculations with the experimental data from NMR spectra measured with and without MAS using either single-pulse excitation (SPE) or the Solomon echo pulse sequence (SE). For δ_{iso} from GIPAW calculations, both $\delta_{iso,DFT,1}$ (eqn (1)) and $\delta_{iso,DFT,2}$ (eqn (2)) are given.

Material	Method	δ_{iso}/ppm	C_Q/MHz	η
KAlH_4	SPE, MAS ²⁵	107.6 ± 0.2	1.29 ± 0.02	0.64 ± 0.02
	SE, static	108 ± 2	1.30 ± 0.02	0.64 ± 0.02
	GIPAW	108.4/107.8	1.69	0.59
NaAlH_4	SPE, MAS ¹⁸	97.5	3.15	0.04
	SPE, MAS	97.2 ± 0.3	3.11 ± 0.03	<0.05
	SPE, static ¹²	101 ± 3	3.08	0
	SPE, static ¹⁹	-	3.10 ± 0.05	0.00 ± 0.05
	SE, static	99 ± 3	3.11 ± 0.02	<0.01
	GIPAW	95.4/96.1	3.14	0

Conclusions

For two complex aluminium hydrides, we have shown that by using the Solomon echo sequence the parameters of the quadrupole coupling can be determined from ^{27}Al NMR spectra measured for stationary samples with at least the same precision as from MAS NMR spectra. For the isotropic chemical shift, the precision of the MAS approach is superior.

The avoidance of mechanical stress and frictional heating caused by fast sample spinning is certainly a great advantage of NMR measurements of stationary samples, in particular when less stable materials are to be investigated.

Furthermore, the Solomon echo sequence can be used with any NMR probe that can generate sufficiently strong rf pulses. Obviously, *in situ* studies of phase transitions or reactions at high pressure in a wide temperature range are easier to accomplish for stationary samples than for those under MAS conditions.

The use of Solomon echoes is of course not limited to ^{27}Al in aluminium hydrides, but should be feasible for other half-integer quadrupolar nuclei with small or moderate quadrupole couplings in materials from various classes of substances, provided that the longitudinal relaxation is slow enough for intense Solomon echoes to be formed.

The encouraging agreement between experimental and GIPAW data obtained is in line with the general notion that modern density functional theory is accurate enough to provide a good description of the electronic structure and hence the efg and quadrupole coupling in a very wide range of solids.⁶⁷

The sensitivity of the quadrupole interaction to the local geometry offers a valuable source of information about the structure. Hence, by determining the parameters of the quadrupole coupling, both from NMR measurements and DFT calculations, it should be possible to distinguish between different structural models for new materials based on diffraction data.

Conflict of interest

There are no conflicts to declare.

Acknowledgement

The authors thank Dr Michael Felderhoff, MPI für Kohlenforschung in Mülheim an der Ruhr, for the preparation of the aluminium hydride samples used. MF gratefully acknowledges funding by the Deutsche Forschungsgemeinschaft (German Research Foundation, DFG) through a Heisenberg fellowship (project no. 455871835).

Supporting Information

Supporting Information is available.

ORCID

Bodo Zibrowius: 0000-0002-3894-7318

Michael Fischer: 0000-0001-5133-1537

References

- (1) Bogdanović, B.; Schwickardi, M. *J. Alloys Compd.* **1997**, *253–254*, 1–9.
- (2) Schüth, F.; Bogdanović, B.; Felderhoff, M. *Chem. Commun.* **2004**, 2249–2258.
- (3) Orimo, S.; Nakamori, Y.; Eliseo, J. R.; Züttel, A.; Jensen, C. M. *Chem. Rev.* **2007**, *107*, 4111–4132.
- (4) Bogdanović, B.; Felderhoff, M.; Streukens, G. *J. Serb. Chem. Soc.* **2009**, *74*, 183–196.
- (5) Frankcombe, T. J. *Chem. Rev.* **2012**, *112*, 2164–2178.
- (6) Li, L.; Xu, C.; Chen, C.; Wang, Y.; Jiao, L.; Yuan, H. *Int. J. Hydrogen Energy* **2013**, *38*, 8798–8812.
- (7) Callini, E. et al. *Appl. Phys. A* **2016**, *122*, 353.
- (8) Milanese, C.; Garroni, S.; Gennari, F.; Marini, A.; Klassen, T.; Dornheim, M.; Pistidda, C. *Metals* **2018**, *8*, 567.
- (9) Suárez-Alcántara, K.; Tena-Garcia, J. R.; Guerrero-Ortiz, R. *Materials* **2019**, *12*, 2724.
- (10) Zhao, L.; Xu, F.; Zhang, C.; Wang, Z.; Ju, H.; Gao, X.; Zhang, X.; Sun, L.; Liu, Z. *Prog. Nat. Sci.: Mater.* **2021**, *31*, 165–179.

- (11) Kellberg, L.; Bildsøe, H.; Jakobsen, H. J. *J. Chem. Soc., Chem. Commun.* **1990**, 1294–1295.
- (12) Tarasov, V. P.; Kirakosyan, G. A. *Russ. J. Inorg. Chem.* **1997**, *42*, 1223–1227.
- (13) Tarasov, V. P.; Bakum, S. I.; Novikov, A. V. *Russ. J. Inorg. Chem.* **2000**, *45*, 1890–1896.
- (14) Bogdanović, B.; Felderhoff, M.; Germann, M.; Härtel, M.; Pommerin, A.; Schüth, F.; Weidenthaler, C.; Zibrowius, B. *J. Alloys Compd.* **2003**, *350*, 246–255.
- (15) Wiench, J.; Balema, V. P.; Pecharsky, V. K.; Pruski, M. *J. Solid State Chem.* **2004**, *177*, 648–653.
- (16) Hwang, S.-J.; Bowman, R. C.; Graetz, J.; Reilly, J. J.; Langley, W.; Jensen, C. M. *J. Alloys Compd.* **2007**, *446–447*, 290–295.
- (17) Kabbour, H.; Ahn, C. C.; Hwang, S.-J.; Bowman, R. C.; Graetz, J. *J. Alloys Compd.* **2007**, *446–447*, 264–266.
- (18) Zhang, J.; Pilette, M.-A.; Cuevas, F.; Charpentier, T.; Mauri, F.; Latroche, M. *J. Phys. Chem. C* **2009**, *113*, 21242–21252.
- (19) Verkuijlen, M. H. W.; van Bentum, P. J. M.; van Eck, E. R. H.; Lohstroh, W.; Fichtner, M.; Kentgens, A. P. M. *J. Phys. Chem. C* **2009**, *113*, 15467–15472.
- (20) Verkuijlen, M. H. W.; Gao, J.; Adelhelm, P.; van Bentum, P. J. M.; de Jongh, P. E.; Kentgens, A. P. M. *J. Phys. Chem. C* **2010**, *114*, 4683–4692.
- (21) Verkuijlen, M. H. W.; van Bentum, P. J. M.; Zabara, O.; Fichtner, M.; Kentgens, A. P. M. *J. Phys. Chem. C* **2011**, *115*, 13100–13106.
- (22) Krech, D.; Zibrowius, B.; Weidenthaler, C.; Felderhoff, M. *Eur. J. Inorg. Chem.* **2014**, 5683–5688.

- (23) Nielsen, T. K.; Javadian, P.; Polanski, M.; Besenbacher, F.; Bystrzycki, J.; Skibsted, J.; Jensen, T. R. *Nanoscale* **2014**, *6*, 599–607.
- (24) Ares, J. R.; Zhang, J.; Charpentier, T.; Cuevas, F.; Latroche, M. *J. Phys. Chem. C* **2016**, *120*, 21299–21308.
- (25) Zibrowius, B.; Felderhoff, M. *Phys. Chem. Chem. Phys.* **2019**, *21*, 12576–12584.
- (26) Freude, D.; Haase, J. In *NMR Basic Principles and Progress*; Diehl, P., Fluck, E., Guenther, H., Kosfeld, R., Seelig, J., Eds.; Springer Verlag: Berlin, 1993; Vol. 29; Chapter Quadrupole Effects in Solid-State Nuclear Magnetic Resonance, pp 1–90.
- (27) Mamatha, M.; Bogdanović, B.; Felderhoff, M.; Pommerin, A.; Schmidt, W.; Schüth, F.; Weidenthaler, C. *J. Alloys Compd.* **2006**, *407*, 78–86.
- (28) Ortmeyer, J.; Bodach, A.; Sandig-Predzymirska, L.; Zibrowius, B.; Mertens, F.; Felderhoff, M. *ChemPhysChem* **2019**, *20*, 1360–1368.
- (29) Freude, D.; Haase, J. Quadrupole Effects in Solid-state NMR, Basic Principles and Experimental Techniques for Nuclei with Half-integer Spins. www.quad-nmr.de, (2013–2022).
- (30) Man, P. P. In *Encyclopedia of Nuclear Magnetic Resonance*; Harris, R. K., Wasylishen, R. E., Eds.; John Wiley & Sons Ltd: Chichester, 2011; Chapter Quadrupolar Interactions, DOI: 10.1002/9780470034590.emrstm0429.pub2.
- (31) Solomon, I. *Phys. Rev.* **1958**, *110*, 61–65.
- (32) Man, P. P. *J. Chem. Phys.* **1997**, *106*, 3908–4444.
- (33) Man, P. P. In *Encyclopedia of Analytical Chemistry*; Meyers, R. A., Ed.; John Wiley & Sons Ltd: Chichester, 2000; Chapter Quadrupole Couplings in Nuclear Magnetic Resonance, General, pp 12224–12265.

- (34) Azais, T.; Bonhomme, C.; Bonhomme-Coury, L.; Vaissermann, J.; Millot, Y.; Man, P. P.; Bertani, P.; Hirschinger, J.; Livage, J. *J. Chem. Soc., Dalton Trans.* **2002**, 609–618.
- (35) Perras, F. A.; Bryce, D. L. *J. Phys. Chem. C* **2012**, *116*, 19472–19482.
- (36) Bonhomme, C.; Gervais, C.; Babonneau, F.; Coelho, C.; Pourpoint, F.; Azais, T.; Ashbrook, S. E.; Griffin, J. M.; Yates, J. R.; Mauri, F.; Pickard, C. J. *Chem. Rev.* **2012**, *112*, 5733–5779.
- (37) Bonhomme, C.; Azais, T. *C. R. Chimie* **2004**, *7*, 417–424.
- (38) Man, P. P. *Solid State Nucl. Magn. Reson.* **1992**, *1*, 149–158.
- (39) Hoult, D. I.; Richards, R. E. *Proc. R. Soc. Lond. A* **1975**, *344*, 311–340.
- (40) Kunwar, A. C.; Turner, G. L.; Oldfield, E. *J. Magn. Reson.* **1986**, *69*, 124–127.
- (41) Clark, S. J.; Segall, M. D.; Pickard, C. J.; Hasnip, P. J.; Probert, M. I. J.; Refson, K.; Payne, M. C. *Z. Kristallogr.* **2005**, *220*, 567–570.
- (42) Milman, V.; Refson, K.; Clark, S.; Pickard, C.; Yates, J.; Gao, S.-P.; Hasnip, P.; Probert, M.; Perlov, A.; Segall, M. *J. Molec. Struct.: THEOCHEM* **2010**, *954*, 22–35.
- (43) Perdew, J. P.; Burke, K.; Ernzerhof, M. *Phys. Rev. Lett.* **1996**, *77*, 3865–3868.
- (44) Hauback, B. C.; Brinks, H. W.; Jensen, C. M.; Murphy, K.; Maeland, A. J. *J. Alloys Compd.* **2003**, *358*, 142–145.
- (45) Ozolins, V.; Majzoub, E.; Udovic, T. *J. Alloys Compd.* **2004**, *375*, 1–10.
- (46) Hauback, B. C.; Brinks, H. W.; Heyn, R. H.; Blom, R.; Fjellvåg, H. *J. Alloys Compd.* **2005**, *394*, 35–38.
- (47) Pickard, C. J.; Mauri, F. *Phys. Rev. B* **2001**, *63*, 245101.

- (48) Profeta, M.; Mauri, F.; Pickard, C. J. *J. Am. Chem. Soc.* **2003**, *125*, 541–548.
- (49) Yates, J. R.; Pickard, C. J.; Mauri, F. *Phys. Rev. B* **2007**, *76*, 024401.
- (50) Yates, J. R.; Dobbins, S. E.; Pickard, C. J.; Mauri, F.; Ghi, P. Y.; Harris, R. K. *Phys. Chem. Chem. Phys.* **2005**, *7*, 1402–1407.
- (51) Ashbrook, S. E.; McKay, D. *Chem. Commun.* **2016**, *52*, 7186–7204.
- (52) Sturniolo, S.; Green, T. F.; Hanson, R. M.; Zilka, M.; Refson, K.; Hodgkinson, P.; Brown, S. P.; Yates, J. R. *Solid State Nucl. Magn. Reson.* **2016**, *78*, 64–70.
- (53) Hauback, B. C.; Brinks, H. W.; Fjellvåg, F. *J. Alloys Compd.* **2002**, *346*, 184–189.
- (54) Brinks, H. W.; Hauback, B. C. *J. Alloys Compd.* **2003**, *354*, 143–147.
- (55) Brinks, H. W.; Hauback, B. C.; Jensen, C. M.; Zidan, R. *J. Alloys Compd.* **2005**, *392*, 27–30.
- (56) Løvvik, O. M.; Opalka, S. M.; Brinks, H. W.; Hauback, B. C. *Phys. Rev. B* **2004**, *69*, 134117.
- (57) Løvvik, O. M.; Opalka, S. M.; Brinks, H. W.; Hauback, B. C. *Phys. Rev. B* **2005**, *71*, 059902(E).
- (58) Balema, V. P.; Pecharsky, V. K.; Dennis, K. W. *J. Alloys Compd.* **2000**, *313*, 69–74.
- (59) Freude, D. In *Encyclopedia of Analytical Chemistry*; Meyers, R. A., Ed.; John Wiley & Sons Ltd: Chichester, 2000; Chapter Quadrupolar Nuclei in Solid-state Nuclear Magnetic Resonance, pp 12188–12224.
- (60) Samoson, A. *Chem. Phys. Lett.* **1985**, *119*, 29–32.
- (61) Taylor, P. C.; Baugher, J. F.; Kriz, H. M. *Chem. Rev.* **1975**, *75*, 203–240.
- (62) Mason, J. *Solid State Nucl. Magn. Reson.* **1993**, *2*, 285–288.

- (63) Brus, J. *Solid State Nucl. Magn. Reson.* **2000**, *16*, 151–160.
- (64) Antonijevic, S.; Bodenhausen, G. *Angew. Chem. Int. Ed.* **2005**, *44*, 2935–2938.
- (65) Pyykkö, P. *Mol. Phys.* **2018**, *116*, 1328–1338.
- (66) Aerts, A.; Brown, A. *J. Chem. Phys.* **2019**, *150*, 224302.
- (67) Zwanziger, J. W. In *NMR of Quadrupolar Nuclei in Solid Materials*; Wasylshen, R. E., Ashbrook, S. E., Wimperis, S., Eds.; Wiley, Chichester, 2012; Chapter Computing Electric Field Gradient Tensors, pp 199–209.